The First Implementation of Respiratory Triggered 4DCBCT on a Linear Accelerator

Ricky T O'Brien[1], Benjamin J Cooper[1,2], Chun-Chien Shieh[1], Uros Stankovic[3], Paul J Keall[1] and Jan-Jakob Sonke[3]

[1]Radiation Physics Laboratory, Sydney Medical School, The University of Sydney, NSW 2006, Australia. [2]Department of Medical Physics, The Canberra Hospital, ACT 2605, Australia. [3]Department of Radiation Oncology, The Netherlands Cancer Institute, Amsterdam 1066CX, The Netherlands.

E-mail: ricky.obrien@sydney.edu.au

Abstract.
Four Dimensional Cone Beam Computed Tomography (4DCBCT) is an image guidance strategy used for patient positioning in radiotherapy. In conventional implementations of 4DCBCT, a constant gantry speed and a constant projection pulse rate are used. Unfortunately, this leads to higher imaging doses than are necessary because a large number of redundant projections are acquired. In theoretical studies, we have previously demonstrated that by suppressing redundant projections the imaging dose can be reduced by 40-50% for a majority of patients with little reduction in image quality. The aim of this study was to experimentally realise the projection suppression technique, which we have called Respiratory Triggered 4DCBCT (RT-4DCBCT).

A real-time control system was developed that takes the respiratory signal as input and computes whether to acquire, or suppress, the next projection trigger during 4DCBCT acquisition. The CIRS dynamic thorax phantom was programmed with a 2cm peak-to-peak motion and periods ranging from 2 to 8 seconds. Image quality was assessed by computing the edge response width of a 3cm imaging insert placed in the phantom as well as the signal to noise ratio of the phantoms tissue and the contrast to noise ratio between the phantoms lung and tissue. The standard deviation in the Superior-Inferior direction of the 3cm imaging insert was used to assess intra-phase bin displacement variations with a higher standard deviation implying more motion blur.

The 4DCBCT imaging dose was reduced by 8.6%, 41%, 54%, 70% and 77% for patients with 2, 3, 4, 6 and 8 second breathing periods respectively when compared to conventional 4DCBCT. The standard deviation of the intra-phase bin displacement variation of the 3cm imaging insert was reduced by between 13% and 43% indicating a more consistent position for the projections within respiratory phases. For the 4 second breathing period, the edge response width was reduced by 39% (0.8mm) with only a 6-7% decrease in the signal to noise and contrast to noise ratios.

RT-4DCBCT has been experimentally realised and reduced to practice on a linear accelerator with a measurable imaging dose reductions over conventional 4DCBCT and little degradation in image quality.

1. Introduction

4DCBCT was first published and implemented between 2003 and 2005 for a fast rotating gantry (Taguchi 2003) and a slow rotating gantry (Sonke et al. 2005). The first commercial release of 4DCBCT was by Elekta in 2009 and then by Varian Medical Systems in 2014. For conventional 4DCBCT, a constant gantry speed and constant projection pulse rate are used so that medically useful images can be obtained for a wide range of patient breathing rates. Unfortunately, the constant gantry speed and constant projection pulse rate lead to both oversampling in the imaging space, which is demonstrated in Figure 1, and streaking artefacts for irregular breathing patients.

To overcome the problems associated with projection oversampling, Respiratory Triggered 4DCBCT (RT-4DCBCT) has been proposed which acquires a single projection per respiratory phase in each breathing cycle (Cooper et al. 2013, Cooper et al. 2015). In simulated studies, with only a small change in image quality, RT-4DCBCT reduces the imaging dose by approximately 50% for sinusoidal breathing traces (Cooper et al. 2013) and an average of 53% for 111 breathing traces acquired from lung cancer patients (Cooper et al. 2015). The aim of this work was to reduce these simulation studies to practice on a linear accelerator.

Implementing RT-4DCBCT on a linear accelerator involves either suppressing projection triggers to the kV source or directly triggering projections. Suppressing alternate projection triggers has previously been implemented for MV scatter correction on Elekta linear accelerators (van Herk et al. 2011). Additionally, when acquiring CBCT scans concurrent with VMAT the Elekta system suppresses projections to aim for a known gantry angle increment. Because of the amount of testing that projection suppression has received on the Elekta system, we have modified the approach used for MV scatter correction by (van Herk et al. 2011) for this study. Directly triggering projections on a Siemens linear accelerator is possible (Fast et al. 2013) but this approach could not be utilised in this study because it requires in house software and Siemens have withdrawn from the linear accelerator market.

2. Method

Conventional linear accelerators are not equipped with a software interface to suppress projection triggers so modifications to the hardware were required. The modifications were performed on the research Elekta Synergy linear accelerator at the Netherlands Cancer Institute and were further tested on a clinical machine. For all image acquisitions a four minute full fan scan of 180° plus the fan angle with projections acquired at 5.5Hz, 120 kV, 20mA, 0.8mm^2 pixels and a 20ms exposure time. This represents one of the clinical acquisition protocols commonly used on Elekta linear accelerators.

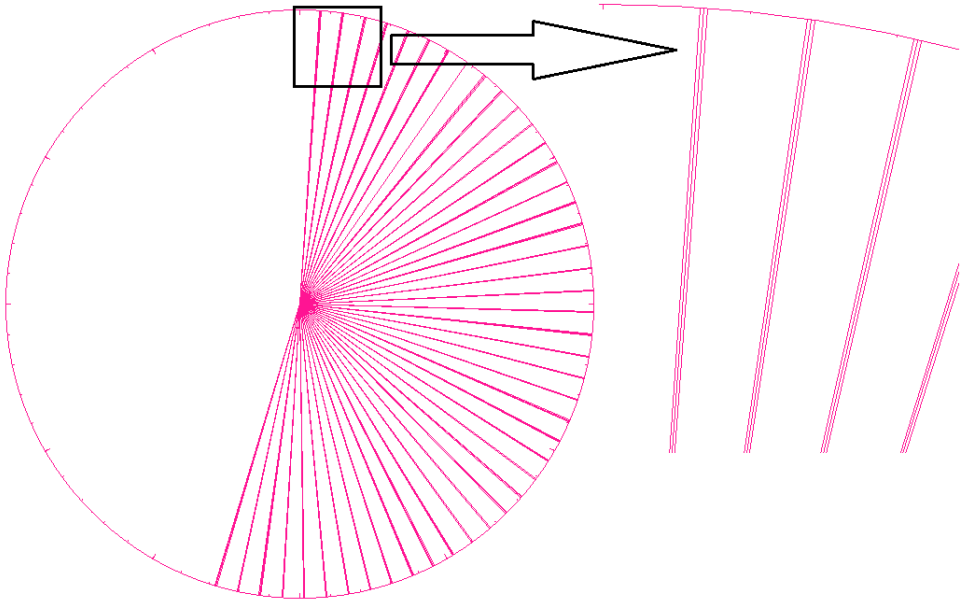

Figure 1. A polar plot of the gantry angle of each projection acquired in a mid inhale phase bin during 4DCBCT acquisition. For this patient there are 45 clusters and 132 projections in total. RT-4DCBCT only acquires one projection per cluster for 45 projections in total. The clustered (redundant) projections provide similar anatomical information and expose the patient to a higher radiation dose than is necessary.

2.1. Suppressing Projections

Projection triggers are sent to the kV source and are synchronised with the kV detector readout with this process schematically represented in Figure 2. Photographs of the experimental equipment are given in Figure 3. The triggers are a TTL pulse sent on a BNC cable which is high, 3.3 volts, for a period of 5ms and then low, 0 volts, for the remaining 176.8ms. An interrupt port on a micro processor was used to detect the rising edge of the TTL pulse with sub millisecond accuracy. An electromagnetic relay was placed in series with the TTL signal and was used to selectively suppress, or absorb, projection triggers based on the patient's real-time respiratory signal. When the relay was closed, a path existed for the TTL pulse to reach the kV source and a projection was acquired. When the relay was open, there was no path for the TTL signal to reach the kV source and the detector read a dark frame which was discarded from image reconstruction.

To avoid issues with the finite closing and opening times of the relay, the relay was not opened or closed within 5ms of a projection pulse. The decision on when to open or close the relay was made by attempting to acquire the closest projection to the centre of each respiratory bin. For each projection, the respiratory signal was predicted to the next projection (i.e. 181.8ms ahead) using linear extrapolation of the signal. If the next projection was predicted to be closer to the centre of the bin than the first projection, then the relay remained open until the next projection where the procedure was repeated. A flowchart of the algorithm controlling image acquisition is given in

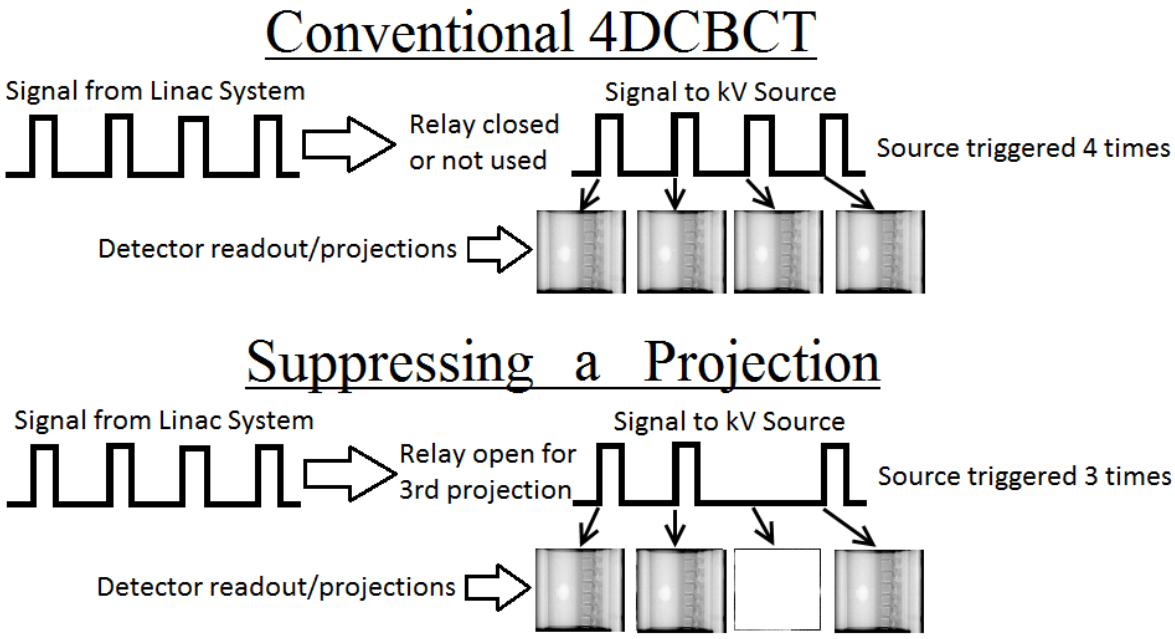

Figure 2. Suppressing kV triggers with a relay. A schematic of the TTL pulse sent to the kV source which is high for 5ms and low for 176.8ms. The kV source is exposed on receipt of each pulse while the detector continuously reading the panel at 5.5Hz.

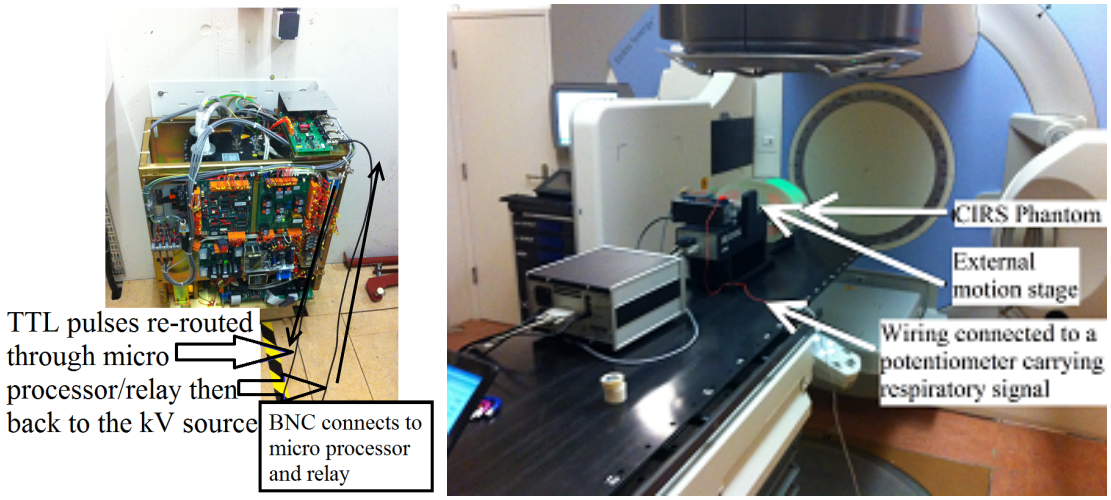

Figure 3. Photographs of the experimental equipment. Left: The BNC cable connections. Right: A photograph of the CIRS phantom.

Figure 4.

2.2. Imaging phantom

The CIRS dynamic thorax phantom model 008A (Computerized Image Reference System Inc, 2428 Almeda Avenue Suite 316, Norfolk, Virginia 23513, USA) was used to represent respiratory motion with the 3cm spherical imaging insert. The in-built sinusoidal breathing traces were used with 2cm peak-to-peak motion (1cm amplitude)

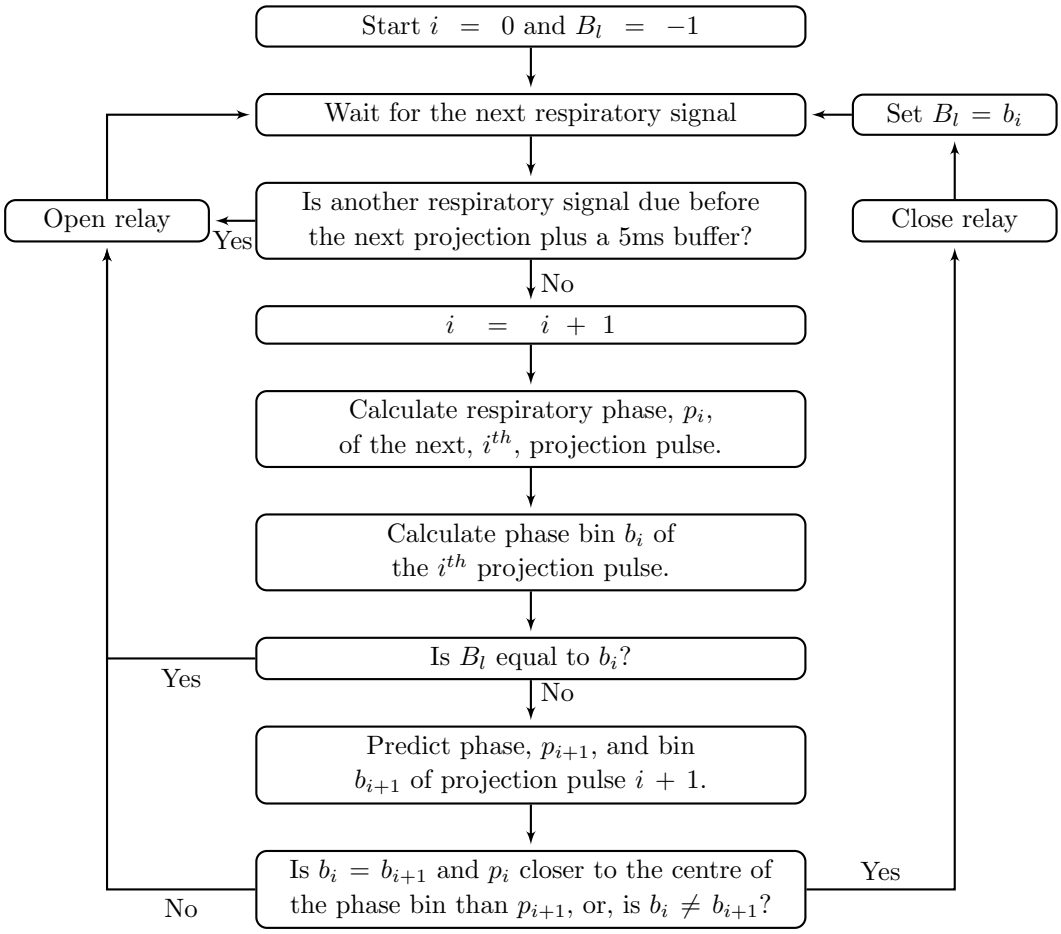

Figure 4. A flowchart showing the main algorithm used on the projection suppression micro processor.

in the superior-inferior direction and respiratory periods of 2, 3, 4, 6 and 8 seconds.

Lujan *et al* (1999) have used breathing traces of the form Cos^{2n} ($n = 1, 2, 3, \ldots$) to represent the cases where the patient spends longer in exhale (Lujan et al. 1999). Using higher values of n produces breathing traces that spend longer in exhale with a value of $n = 3$ being a practical upper limit for lung cancer patients (George et al. 2005). We have therefore used $n = 3$ (Cos^6) with a 4 second breathing period to represents a realistic extreme case for patients that spend longer in exhale.

2.3. Respiratory signal and phase calculation

A variety of external devices are used in radiotherapy to detect a respiratory signal such as bellows belts and the Real-Time Position Management (RPM) system from Varian Medical Systems. For this study a linear potentiometer was used to extract a respiratory signal based on the motion of the surrogate platform on the CIRS phantom. The respiratory signal was connected directly to the micro processor that was used to determine when to suppress projection triggers.

A total of ten phase bins were used with the phase rising linearly from peak exhale to peak exhale. The phase bins were further adjusted by half a phase bin so that the exhale and inhale limits were not divided into two phase bins. To avoid the added complication of real-time phase determination in this proof of principle study, a rolling average of the period of the most recent five respiratory signals was used to predict the respiratory phase for one breathing cycle into the future.

2.4. Image reconstruction

Images were reconstructed using the FDK algorithm from the open source Reconstruction Tool Kit (RTK) (Feldkamp et al. 1984) and (Rit et al. 2014). The images were reconstructed with $256 \times 256 \times 256$ voxels of size 1mm^3.

2.5. Determining the system latency

To determine system latencies a second respiratory signal was extracted from the images with the gantry held at a fixed position which was then compared to the external respiratory signal from section 2.3. The second respiratory signal was extracted from the motion of the 3cm imaging insert using the following procedure:

(i) Perform a two dimensional gradient filter on each projection.

(ii) Convert to a black and white gradient image by marking pixels white when the gradient is larger than the mean gradient plus two standard deviations.

(iii) Minimise the normalised cross correlation between the first gradient image and the i^{th} gradient image by moving the i^{th} image up and down.

(iv) Convert the distance moved in pixels to distance moved in millimetres.

The RMS in the difference between the second respiratory signal that was extracted from the images as described in this section and the external signal recorded according to section 2.3 was computed for a range of time delays with the time delay corresponding to the minimum RMS assumed to be the overall system latency. We measured the system latency at 100-120ms for sinusoidal breathing traces with periods of 2, 3, 4, 6 and 8 seconds. The system latency includes a delay in the signal because the potentiometer contact points were not completely rigidly attached which caused the motion of the potentiometer to trail the motion of the CIRS phantom by a small amount. The latency also includes the time required to record, filter and process the respiratory signal. To account for this latency, the respiratory signal was linearly predicted ahead by 110ms for all 4DCBCT acquisitions.

2.6. Intra-phase bin displacement variation

One component of blurring of anatomical features in 4DCBCT images is caused because projections are acquired at different respiratory states within each phase bin. For a patient with a 2cm peak-to-peak breathing motion, on average, each respiratory phase

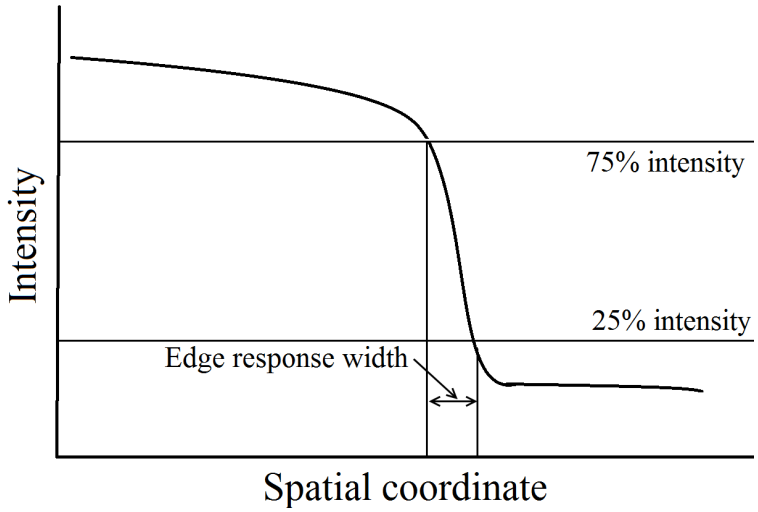

Figure 5. A schematic showing how the edge response width is calculated. A smaller edge response width indicates less motion blur and sharper images.

covers 2mm of motion which will result in some blurring in the reconstructed images. To estimate the intra-phase bin motion, the displacement signal that was extracted from the images was recorded with the standard deviation of the displacement used as an indicator of motion blur. We expect RT-4DCBCT to have a lower intra-phase bin displacement variation than conventional 4DCBCT as we acquire projections closer to the centre of each phase bin.

2.7. Signal to noise ratio (SNR) and Contrast to Noise Ratio (CNR)

We have used the signal to noise ratio (SNR), which was calculated by dividing the mean intensity by the standard deviation of the voxels in a 1cm^3 region of tissue in the reconstructed CIRS phantom images:

$$SNR = \bar{I}_{tissue}/\sigma_{tissue},$$

where $\bar{I}_{tissue}$ and σ_{tissue} are the mean and standard deviation of the voxels intensities in a 1cm^3 region of tissue in the reconstructed CIRS phantom images.

The contrast to noise ratio was calculated by computing the difference between the mean lung and tissue intensities and dividing by the standard deviation of the lung in 1cm^3 regions of the tissue and lung respectively:

$$CNR = |\bar{I}_{tissue} - \bar{I}_{lung}|/\sigma_{tissue},$$

where $\bar{I}_{lung}$ is the mean voxels intensity in a 1cm^3 region of the lung in the reconstructed CIRS phantom images. A higher value of the SNR and CNR indicates that there is less noise or higher contrast in the reconstructed image respectively.

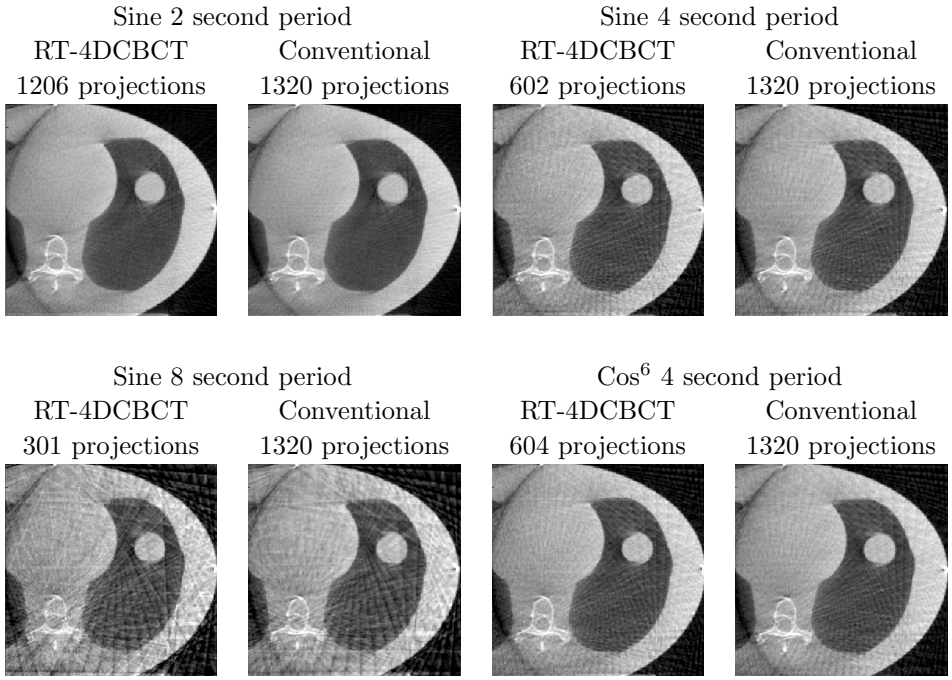

Figure 6. A axial slice of the reconstructed images with conventional 4DCBCT and RT-4DCBCT at peak inhale. Visually there is very little difference in image quality between the two 4DCBCT methods.

2.8. Edge response width (Image sharpness)

For the 4DCBCT acquisitions, the images were reconstructed and the sharpness of the image was quantified using the edge response width (ERW), see Figure 5. Specifically, the axial slice was selected where the imaging insert was at its maximum diameter of 3cm and the ERW was calculated across the edge of the imaging insert using 75% and 25% as the cut-off intensity thresholds. To reduce the impact that streaking artefacts have on the ERW, we averaged the ERW over both sides of the 3cm imaging insert for all phase bins to give an average and standard deviation for the ERW.

3. Results

3.1. Reconstructed images

Figure 6 displays one slice at peak inhale for four different respiratory patterns. Visually, there is little difference between the reconstructed images from conventional 4DCBCT and RT-4DCBCT despite a significant reduction in the number of projections, and associated imaging dose, used to reconstruct the images. For the eight second breathing periods there are approximately 30 projections per respiratory phase and streaking artefacts noticeably degrade the image quality.

Table 1. The number of images and the average standard deviation across the 10 respiratory bins of the 3cm imaging inserts displacement. A value of 0mm indicates that the imaging insert was at exactly the same location for each projection acquired.

	RT-4DCBCT		Conventional 4DCBCT	
Breathing Trace	Number of Projections	Average SD (mm)	Number of Projections	Average SD (mm)
Sin 2 seconds	1206	0.7	1320	1.1
Sin 3 seconds	791	0.7	1319	1.0
Sin 4 seconds	602	0.4	1320	0.7
Sin 6 seconds	401	0.5	1319	0.7
Sin 8 seconds	301	0.4	1320	0.7
Cos^6 4 seconds	604	0.4	1320	0.7

3.2. Intra-phase bin displacement variation

Table 1 gives the total number of projections acquired as well as the mean and standard deviation of the intra-phase bin displacement variation that was extracted from the motion of the 3cm imaging insert. The intra-phase bin displacement variation is reduced with RT-4DCBCT indicating that projections are acquired in a more consistent respiratory state than for conventional 4DCBCT. Note that the intra-phase bin displacement variation does not drop below 0.4mm which indicates that this is the maximum accuracy of our method when taking into account the errors caused by: (1) The segmentation of the marker, (2) Noise in the respiratory signal, (3) Errors calculating the real-time phase and prediction errors and (4) The pixel size. For the 2 and 3 second breathing periods, the larger intra-phase bin displacement variations were caused by a higher rate of noise in our external respiratory signal which led to small errors in determining the real-time phase. For individual respiratory phases, the intra-phase displacement variation was smaller in the inhale and exhale limit phase with values below 0.5mm and rising to between 1mm and 3.5mm, depending on the breathing rate, for the mid inhale phase bins.

3.3. Signal to noise and contrast to noise ratios: Image noise

Figure 7 displays the mean and standard deviation of the signal to noise and contrast to noise ratios for the 4DCBCT reconstructions. The results indicate that SNR and CNR are marginally degraded with RT-4DCBCT when compared to conventional 4DCBCT. The reduction is only small indicating that streaking artefacts dominate over statistical noise which is evident in the 2 second breathing period data where fewer streaks lead to a higher SNR and CNR.

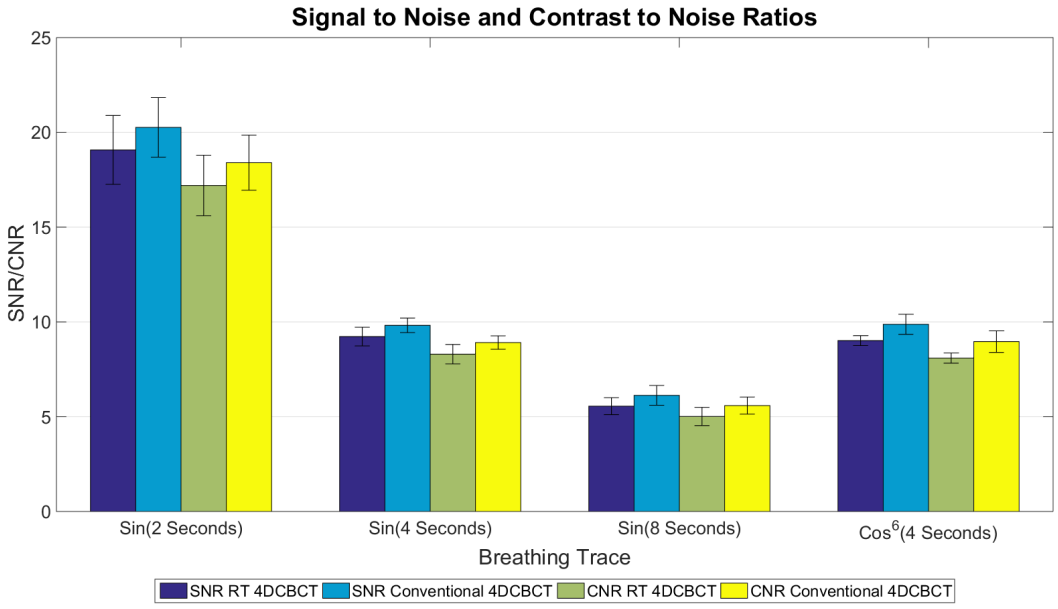

Figure 7. The mean and standard deviation of the signal to noise and contrast to noise ratios across the 10 phase bins for a variety of sinusoidal and cosine breathing traces with conventional 4DCBCT and RT-4DCBCT.

3.4. Edge response width: Image sharpness

Figure 8 displays the mean and standard deviation of the edge response width in both the left-right (LR) and superior-inferior direction (SI). There was no motion of the phantom in the AP or LR direction, so the LR values indicate the smallest achievable edge response width that is expected from our simulations in the SI, AP and LR directions. For the eight second breathing period, streaking artefacts caused by the large gaps between projection clusters has made the standard deviation in the edge response width much larger than all of the other breathing periods. As the edge response width is dominated by streaking artefacts for the eight second breathing period, which can be variable from patient to patient, it is hard to draw any concrete conclusions from the edge response width for eight second breathing periods or larger. For the patient with a two second breathing period, there does not appear to be a significant reduction in the LR edge response width when comparing to the patient with a four second breathing period, which suggests that the extra projections acquired for the two second breathing period do not significantly improve the edge response width.

In the SI direction there is a measurable decrease in the edge response width when using RT-4DCBCT compared to conventional 4DCBCT. For the sine breathing trace with a four second breathing period, the standard deviation in the edge response width in SI is more than halved from 0.7mm to 0.3mm and the mean edge response width is reduced from 2.1mm to 1.3mm. For the two second breathing period, the edge response width is not significantly reduced because only 8.6% of projections were suppressed

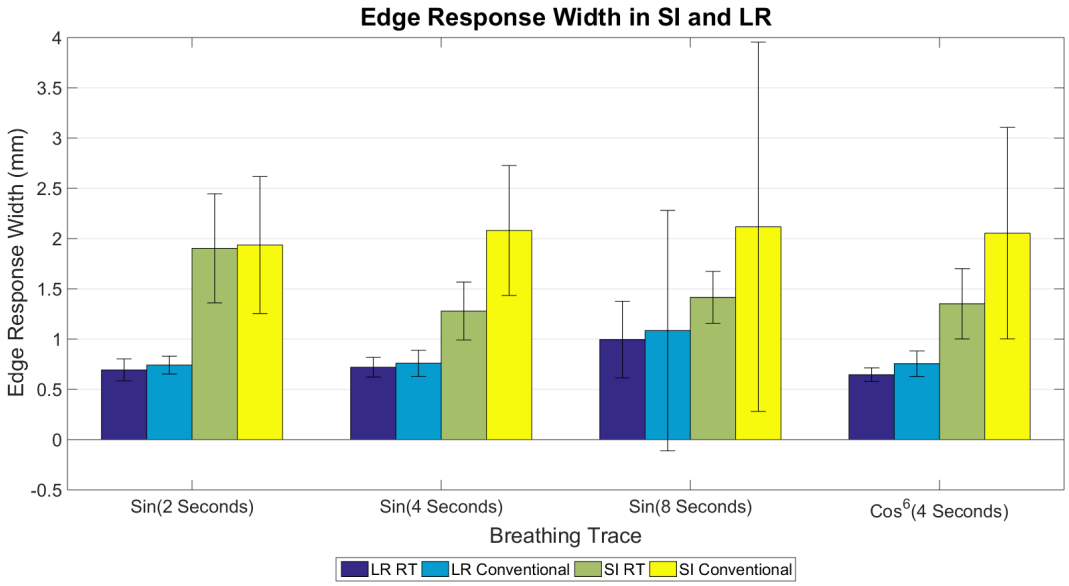

Figure 8. The mean and standard deviation across the 10 phase bins of the edge response width in the SI and LR directions for conventional 4DCBCT and RT-4DCBCT. A lower edge response width indicates a sharper image. In the SI direction, the edge response width is increased due to blurring as a result of intra-phase bin displacement variations. The edge response width in LR is fairly consistent between conventional and RT 4DCBCT, but it has been improved considerably for RT 4DCBCT in the SI direction.

with RT-4DCBCT. Similar to the intra-phase displacement variation, the edge response width at peak exhale and peak inhale is smaller than the mid inhale phase bins.

4. Discussion

We have experimentally realised a technique to selectively suppress projections during 4DCBCT acquisition on a linear accelerator with a measurable improvement in image sharpness and a substantial reduction in the imaging dose. Although the technique requires an external relay and micro processor, the technique is simple to implement on Elekta linear accelerators. In addition, no changes to the existing clinical protocols and work flows will be required to implement the technique which aids rapid translation to clinical practice.

Although the focus of RT-4DCBCT is to reduce imaging dose, our results suggest that image sharpness can potentially be improved by selectively suppressing projections which could be explored in more detail with patient data to see if there is an image quality benefit. It should be pointed out that these benefits may not translate to actual patient images for several reasons: (1) There are variations in the patient's anatomy from breathing cycle to breathing cycle for the same displacement and these variations may be larger than any improvement in image sharpness that was observed in this study.

(2) Phase binning is currently used clinically which is known to contain larger errors when compared to displacement binning for 4DCT (Abdelnour et al. 2007). (3) The focus of many iterative reconstruction methods is to reduce streaking artefacts caused by a poor angular distribution of projections and these errors lead to larger errors than the image sharpness errors that we have observed.

The Elekta system has a fixed frame rate of 5.5Hz and our results suggest that for fast breathing patients, i.e. a 2 second period, there are less than 10% of projections suppressed. These results suggest that a higher frame rate, such as the 10-15Hz achievable with Varian linear accelerators, could improve image sharpness further. The average breathing period for lung cancer patients has been measured to be 3.8 seconds (5th and 95th percentile range 2.1-6.7 s) (George et al. 2005). The estimated dose reduction for this population ranges from 8.6% to 66% with the average patient, who has a 3.8s breathing period, having a dose reduction of around 50%.

Our work has focussed on reducing the imaging dose during 4DCBCT acquisition which is in line with the ALARA principle (As Low As Reasonably Achievable) and the Image Wisely/Image Gently campaigns (Brink & Amis 2010) and (Goske et al. 2008). In addition to the imaging dose reduction, the improvement in image sharpness was a surprising bonus for the technique. To address image quality issues further, regulating the gantry speed in response to the patient's real-time respiratory signal is a logical extension to this method (O'Brien et al. 2013) and (O'Brien, Cooper, Kipritidis, Shieh & Keall 2014). Various other techniques exist to address the image quality in conjunction with RT-4DCBCT including iterative reconstruction techniques, (Bian et al. 2010), (Bergner et al. 2010), (Leng et al. 2008), (Li et al. 2007), (Brehm et al. 2012), (Brehm et al. 2012), and projection sorting techniques (O'Brien, Kipritidis, Shieh & Keall 2014).

One challenge with RT-4DCBCT is that real-time phase information is required. Real-time phase algorithms are commercially available in radiotherapy gating systems and respiratory sensors. RT-4DCBCT has been realistically simulated with the real-time phase signal that comes directly off the Varian RPM system for 111 breathing traces acquired from lung cancer patients (Cooper et al. 2015). Despite the RPM real-time phase being unstable, it was demonstrated that RT-4DCBCT reduces the average imaging dose by 53% across the patient cohort (Cooper et al. 2015). A further real-time phase algorithm has been published by (Ruan et al. 2009) which has been used to simulate both gantry control and projection suppression during 4DCBCT acquisition for breathing traces acquired from lung cancer patients (O'Brien, Cooper, Kipritidis, Shieh & Keall 2014). It was demonstrated that the Ruan method outperforms the Varian RPM method because there are fewer sudden changes in the phase signal (O'Brien, Cooper, Kipritidis, Shieh & Keall 2014). Using the Ruan method on a 3GHz desktop, the computation time for each new respiratory signal is 1-2 milliseconds. However, on our 168Mhz microcontroller, the computation time was more than 0.5s, so a dedicated CPU to compute phase will be needed for commercial implementation; the development of this system is beyond the scope of this study.

Several additional approaches to eliminate, or improve, real-time phase calculations

are possible, such as: (1) To improve the accuracy of the real-time phase calculation, an internal-external correlation model could be used that is updated as new images are acquired (Low et al. 2005) and (Ionascu et al. 2007). (2) Displacement binned 4DCBCT could be developed to overcome the need to compute phase in real-time. (3) In the absence of an external respiratory monitoring system, a patient specific frame rate could be investigated to reduce the imaging dose.

5. Conclusions

This is the first implementation of respiratory triggered 4DCBCT on a linear accelerator. RT-4DCBCT is an effective method to reduce 4DCBCT imaging dose with little change to clinical protocols, a measurable improvement in image sharpness and little degradation to image quality.

Acknowledgements and Disclosures

Professor Keall would like to acknowledge the support of a National Health and Medical Research Council (NHMRC) Australia Fellowship. This project was supported by a Cancer Australia Priority Driven Collaborative Cancer Research Scheme project grant number 1084566 and in part by NHMRC project grant 1034060. Dr Sonke would like to acknowledge research support from Elekta and that his department receives licensing fees from Elekta.

References

Abdelnour A F, Nehmeh S A, Pan T, Humm J L, Vernon P, Schoder H, Rosenzweig K E, Mageras G S, Yorke E, Larson S M & Erdi Y E 2007 *Phys Med Biol* **52**(12), 3515–29.

Bergner F, Berkus T, Oelhafen M, Kunz P, Pa T, Grimmer R, Ritschl L & Kachelriess M 2010 *Med Phys* **37**(9), 5044–53.

Bian J, Siewerdsen J H, Han X, Sidky E Y, Prince J L, Pelizzari C A & Pan X 2010 *Phys Med Biol* **55**(22), 6575–99.

Brehm M, Paysan P, Oelhafen M, Kunz P & Kachelriess M 2012 *Medical Physics* **39**(12), 7603–7618.

Brink J A & Amis E S 2010 *Radiology* **257**(3), 601–602.

Cooper B J, O'Brien R T, Balik S, Hugo G D & Keall P J 2013 *Med Phys* **40**(4), 041901.

Cooper B J, O'Brien R T, Kipritidis J, Shieh C C & Keall P J 2015 *Phys Med Biol* **60**(24), 9493–9513.

Fast M, Wisotzky E, Oelfke U & Nill S 2013 *Medical Physics* **40**(9), 091909.

Feldkamp L A, Davis L C & Kress J W 1984 *Journal of the Optical Society of America a-Optics Image Science and Vision* **1**(6), 612–619.

George R, Vedam S S, Chung T D, Ramakrishnan V & Keall P J 2005 *Medical Physics* **32**(9), 2850–2861.

Goske M J, Applegate K E, Boylan J, Butler P F, Callahan M J, Coley B D, Farley S, Frush D P, Hernanz-Schulman M, Jaramillo D, Johnson N D, Kaste S C, Morrison G, Strauss K J & Tuggle N 2008 *American Journal of Roentgenology* **190**(2), 273–274.

Ionascu D, Jiang S B, Nishioka S, Shirato H & Berbeco R I 2007 *Med Phys* **34**(10), 3893–903.

Leng S, Tang J, Zambelli J, Nett B, Tolakanahalli R & Chen G H 2008 *Physics in Medicine and Biology* **53**(20), 5653–5673.

Li T, Koong A & Xing L 2007 *Med Phys* **34**(9), 3688–95.

Low D A, Parikh P J, Lu W, Dempsey J F, Wahab S H, Hubenschmidt J P, Nystrom M M, Handoko M & Bradley J D 2005 *Int J Radiat Oncol Biol Phys* **63**(3), 921–9.

Lujan A E, Larsen E W, Balter J M & Ten Haken R K 1999 *Med Phys* **26**(5), 715–20.

O'Brien R T, Cooper B J & Keall P J 2013 *Phys Med Biol* **58**(6), 1705–23.

O'Brien R T, Cooper B J, Kipritidis J, Shieh C & Keall P J 2014 *Phys Med Biol* **59**(3), 579–95.

O'Brien R T, Kipritidis J, Shieh C C & Keall P J 2014 *Phys Med Biol* **59**(19), 5631–49.

Rit S, Oliva M V, Brousmiche S, Labarbe R, Sarrut D & Sharp G C 2014 *Xvii International Conference on the Use of Computers in Radiation Therapy (Iccr 2013)* **489**.

Ruan D, Fessler J A, Balter J M & Keall P J 2009 *Phys Med Biol* **54**(15), 4777–92.

Sonke J J, Zijp L, Remeijer P & van Herk M 2005 *Medical Physics* **32**(4), 1176–1186.

Taguchi K 2003 *Medical Physics* **30**(4), 640–650.

van Herk M, Ploeger L & Sonke J J 2011 *Radiother Oncol* **100**(3), 365–9.